International Journal of Applied Engineering Research ISSN 0973-4562 Volume 13, Number 6 (2018) pp. 3590-3597

The Numerical Results of a Study of Different Materials by Local Radial Point Interpolation Method (LRPIM)

Jaouad Eddaoudy[1*], Touria Bouziane[2]

[1, 2] Department of physics, Faculty of Sciences, Moulay Ismail University B.P.11201 Meknes, Morocco.

Abstract

In this paper, the LRPIM meshless method is used for the numerical implementation of the equations of an elastostatic 2-D plate problem based on the local Petrov Galerkin method formulation and by using two radial basis functions (RBFs) are: Multi-Quadratic(MQ) and Thin Plate Spline(TPS). We studied the effect of sizing parameters of sub-domains and the parameters of RBFs functions on the accuracy and convergence of the LRPIM method by using the regular distribution of nodes for different materials and by comparison with analytical results and that available from the literatures.

Keywords: Meshless method, Petrov Galerkin method formulation, radial basis functions, shape parameters, sizing parameters, Point Interpolation Method.

INTRODUCTION

In the last decades, many useful meshless methods have been provided to solve partial differential equations, and they are regarded as potential numerical methods in Computational Mechanics and Physics. Radial Basis Functions (RBF) were first applied to solve numerically, partial differential equations in 1990 by Kansa[1], when a technique based on the direct Collocation method and the Multiquadric RBF was used to model dynamic fluids. The direct Collocation procedure used by Kansa is relatively simple to implement, however, it results in asymmetric system of equations due to the mix of governing equations and boundary conditions.

Several meshless methods, such as Smoothed Particle Hydrodynamics Method[2], the Diffuse Element Method[3], the Element-Free Galerkin Method[4, 5],the Reproducing Kernel Particle Method [6], the Partition of Unity Method[7], the Hp-clouds method [8], the finite point method [9], the Meshless Local Petrov–Galerkin method [10], and the general Finite Difference Method [11], have been proposed and achieved remarkable progress in solving a wide range of static and dynamic problems.

The meshless method is used in different works for example, a local Heaviside weighted meshless method for two-dimensional solids using radial basis functions by J. R. Xiao and M. A. McCarthy[12], Meshless and Meshfree by J. S. Chen and T. Belytschko [13], a novel meshless local Petrov–Galerkin method for dynamic coupled thermoelasticity analysis under thermal and mechanical shock loading by Bao-Jing Zheng and al. [14]

Two different types of PIM formulations have been simultaneously developed, the first using the polynomial basis and the radial basis functions (RBFs) and the second method using the pure radial basis functions (RBFs) [15 − 20]. The point interpolation method (PIM) is a MFree interpolation technique that was used by G.R. Liu and al. [21 − 24] to construct shape functions using nodes distributed locally to formulate MFree weak-form methods.

The LRPIM formulation without polynomial for elastic analysis of 2D elastostatic plate proposed in this paper, we solve this problem by using two radial basis functions (RBFs) [26] are; Multi-Quadratic (MQ) [27] and Thin Plate Spline (TPS)[28]. In a meshless (meshfree) method, a set of scattered nodes used instead of meshing the domain of the problem. The most attractive characteristic of the method is that its shape functions are of Kronecker Delta function, and thus the essential boundary condition can be imposed in a straightforward and effective manner.

The organization of this paper is as follows. In Section 2, we describe Local Radial Point Interpolation Method (LRPIM) Formulation.

In Section 3, the Point Interpolation using Radial Basis Functions presented. In Section 4, we give some numerical analysis results for different materials with LRPIM method to support our theoretical discussion. The conclusion presented in Section 5.

LOCAL WEAK FORM OF LRPIM

We consider the following 2D dimensional static problem in linear elasticity on the domain Ω bounded by the boundary Γ:

$$\begin{aligned} \sigma_{ij} + b_i &= 0 && \text{in } \Omega \\ u_i &= \bar{u}_i && \text{at } \Gamma_u \\ \sigma_{ij} n_j &= \bar{t}_i && \text{at } \Gamma_t \end{aligned} \qquad (1)$$

where

σ_{ij}: is the stress tensor,

b_i: the body force,

$\bar{u}_i$: the prescribed displacements on essential boundaryΓ_u,

$\bar{t}_i$: the tractions on natural boundary Γ_t

n_j: the normal direction index.

Note that the global domain is shared by the subdomains and the nodes are regularly distributed over the domain used.

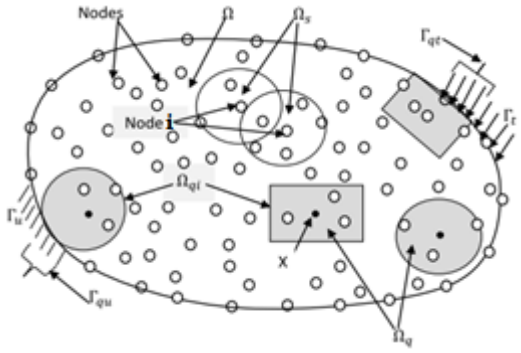

Figure 1: Sub-domains and their boundaries.

where

Γ_{qi}: the internal boundary of the quadrature domain, which does not intersect with the global boundary Γ,

Γ_{qt}: the part of the natural boundary that intersects with the quadrature domain,

Γ_{qu}: the part of the essential boundary that intersects with the quadrature domain.

The local weighted residual form defined over a local quadrature domain Ω_q bounded by Γ_q for each node *i* of the nodal distribution has the following form:

$$\int_{\Omega_q} \theta_i\left(\sigma_{ij,j} + b_i\right) d\Omega - \alpha \int_{\Gamma_{qu}} \theta_i(u_i - \bar{u}_i)d\Gamma = 0 \qquad (2)$$

where the test function θ_i chosen such that they eliminate or simplify the domain integral on Ω_q. This we can use the cubic spline function:

$$\theta_i = \begin{cases} \frac{2}{3} - 4r_i^2 + 8r_i^3, & si\ |r_i| \le \frac{1}{2} \\ \frac{4}{3} - 4r_i + 4r_i^2 - \frac{4}{3}r_i^3, & si\ \frac{1}{2} < |r_i| \le 1 \\ 0 \quad , & si\ |r_i| > 1 \end{cases} \qquad (3)$$

where $r_i = \frac{d_i}{r_w} = \frac{|X - X_i|}{r_w}$

In which $d_i = |X - X_i|$ the distance from node X_i to the sampling point X, and r_w is the size of the support domain for the weight function.

The penalty parameter α is introduced in order to satisfy the geometric boundary condition.

Using $\sigma_{ij,j}\theta_i = (\sigma_{ij}\theta_i)_{,j} - \sigma_{ij}\theta_{i,j}$ and the divergence theorem[24], eq. (2) can be re-written:

$$\int_{\partial\Omega_q} \theta_i\sigma_{ij}n_j\, d\Gamma - \int_{\Omega_q} \theta_{i,j}\sigma_{ij}\, d\Omega + \int_{\Omega_q} \theta_i b_i\, d\Omega - \alpha \int_{\Gamma_{qu}} \theta_i(u_i - \bar{u}_i)d\Gamma = 0 \qquad (4)$$

The boundary $\partial\Omega_q$ for the local quadrature domain Ω_q is composed by three parts (figure 1), i.e.

$$\partial\Omega_q = \Gamma_{qi} \cup \Gamma_{qt} \cup \Gamma_{qu}$$

therefore, eq. (4) can be re-written**:**

$$\int_{\Gamma_{qi}} \theta_i\, \sigma_{ij}n_j\, d\Gamma + \int_{\Gamma_{qt}} \theta_i\sigma_{ij}n_j\, d\Gamma + \int_{\Gamma_{qu}} \theta_i\sigma_{ij}n_j\, d\Gamma - \int_{\Omega_q} \theta_{i,j}\sigma_{ij}\, d\Omega + \int_{\Omega_q} \theta_i b_i\, d\Omega - \alpha \int_{\Gamma_{qu}} \theta_i(u_i - \bar{u}_i)d\Gamma = 0 \qquad (5)$$

For a local quadrature domain located entirely within the global domain, there is no intersection between Γ_q and the global boundary Γ, thus, in this case: $\partial\Omega_q = \Gamma_{qi} = \Gamma_q$ i.e.

there is no integral over Γ_{qu} and Γ_{qt}

$$\int_{\Gamma_q} \theta_i\sigma_{ij}n_j\, d\Gamma - \int_{\Omega_q} \theta_{i,j}\sigma_{ij}\, d\Omega + \int_{\Omega_q} \theta_i b_i\, d\Omega = 0 \qquad (6)$$

Considering the relation between the stress and the traction on the boundary:

$$\sigma_{ij}n_j = t_i \qquad (7)$$

The local weak form eq. (6) is leading to local boundary integral equations:

$$\int_{\Gamma_q} \theta_i t_i\, d\Gamma - \int_{\Omega_q} \theta_{i,j}\, \sigma_{ij}\, d\Omega + \int_{\Omega_q} \theta_i b_i\, d\Omega = 0 \qquad (8)$$

LOCAL RADIAL POINT INTERPOLATION METHOD USING RADIAL BASIS FUNCTIONS

We consider a point $X = (x, y)$ in the local support domain and the continuous function u defined in the problem domain. We use *n* nodes regularly distributed in the local support domain to approximate the value **u**(X)at the point X of function **u** in the form:

$$\mathbf{u}^h(X) = \sum_{i=1}^{n} R_i(X)a_i = \mathbf{R}^T(X)\boldsymbol{a} \qquad (9)$$

where

n: the number of nodes in the local support domain.

$\boldsymbol{a}$: the vector of coefficients defined by

$$\boldsymbol{a}^T = \{a_1, a_2, a_3, \dots, a_n\} \qquad (10)$$

$R_i(X)$: the Radial basis function it is expressed as:

$$R_i(X) = R_i(r_i) = R_i(x, y) \qquad (11)$$

r_i: The distance between point $X = (x, y)$ and node $X_i = (x_i, y_i)$ in a two dimensional problem:

$$r_i = [(x - x_i)^2 + (y - y_i)^2]^{\frac{1}{2}} \qquad (12)$$

The vector **R** has the form:

$$\mathbf{R^T}(\mathrm{X}) = [\mathrm{R}_1(\mathrm{X}), \mathrm{R}_2(\mathrm{X}), \dots, \mathrm{R}_n(\mathrm{X})] \quad (13)$$

We use two radial basis functions as:

Table 1: Typical radial basis functions with dimensionless shape parameters.

Name	Expression	Shape parameters (real number)
1. Multi-quadratic(MQ)	$\mathrm{R_i}(x, y)= (r_i^2+(\alpha_c d_c)^2)^q$	$\alpha_c \geq 0$, q
2. Thin plate spline(TPS)	$\mathrm{R_i}(x, y)=r_i^{\eta}$	η

The coefficients $\mathrm{a_i}$ in eq. (10) are determined by enforcing the interpolated function **u** through all the n nodes within the support domain.

The numerical value at the $\mathrm{k^{th}}$ point of the function **u** has the form:

$$\mathbf{u}_\mathrm{k}(r_k) = \mathbf{u}(\mathrm{x_k}, \mathrm{y_k}) = \sum_{\mathrm{i}=1}^{n} \mathrm{R_i}(\mathrm{x_k}, \mathrm{y_k})\mathrm{a_i}, \mathrm{k} = 1,2, \dots, n \quad (14)$$

where

$$\mathrm{r_k} = [(\mathrm{x_k} - \mathrm{x_i})^2 + (\mathrm{y_k} - \mathrm{y_i})^2]^{\frac{1}{2}}$$

Eq. (9) can be expressed in following matrix form:

$$\mathbf{U} = \mathbf{R_0}\boldsymbol{a} \quad (15)$$

where **U** is the vector that collects all the nodal displacements at the regularly distributed node of the support domain. A unique solution for vector of coefficients $\boldsymbol{a}$ is obtained if the inverse of $\mathbf{R_0}$ exists

$$\boldsymbol{a} = \mathbf{R_0^{-1}}\mathbf{U} \quad (16)$$

Substituting the foregoing equation into eq. (9) leads to:

$$\mathbf{u}^\mathrm{h}(\mathrm{X}) = \mathbf{R}^\mathrm{T}(\mathrm{X})\mathbf{R}_0^{-1}\mathrm{U} = \boldsymbol{\Phi}(\mathrm{X})\mathbf{U} \quad (17)$$

The matrix $\boldsymbol{\Phi}(\mathrm{X})$ of *n* shape functions is

$$\boldsymbol{\Phi}(\mathrm{X}) = [\mathrm{R}_1(\mathrm{X}), \mathrm{R}_2(\mathrm{X}), \mathrm{R}_3(\mathrm{X}) \dots, \mathrm{R}_n(\mathrm{X})]\mathbf{R}_0^{-1}$$

$$\boldsymbol{\Phi}(\mathrm{X}) = [\varphi_1(\mathrm{X}), \varphi_2(\mathrm{X}), \dots, \varphi_\mathrm{k}(\mathrm{X}), \dots, \varphi_n(\mathrm{X})] \quad (18)$$

The approximation for the displacement at a point X can be re-written:

$$\mathbf{u}^\mathrm{h}{}_{(2\times1)}(\mathrm{X}) = \begin{Bmatrix} \mathrm{u} \\ \mathrm{v} \end{Bmatrix}$$

$$\mathbf{u}^\mathrm{h}{}_{(2\times1)}(\mathrm{X}) = \begin{bmatrix} \varphi_1 & 0 & \dots & \varphi_\mathrm{n} & 0 \\ 0 & \varphi_1 & \dots & 0 & \varphi_\mathrm{n} \end{bmatrix} \begin{Bmatrix} u_1 \\ v_1 \\ \vdots \\ u_n \\ v_n \end{Bmatrix}$$

$$\mathbf{u}^\mathrm{h}{}_{(2\times1)}(\mathrm{X}) = \boldsymbol{\Phi}_{(2\times2n)}(\mathrm{X})\mathbf{U}_{(2n\times1)} \quad (19)$$

The strains can be obtained by using the approximated displacements:

$$\boldsymbol{\varepsilon}_{(3\times1)} = \mathbf{L}\mathbf{u}^\mathrm{h} = \mathbf{L}_{(3\times2)}\boldsymbol{\Phi}_{(2\times2n)}\mathbf{U}_{(2n\times1)} \quad (20)$$

$$\boldsymbol{\varepsilon}_{(3\times1)} = \begin{bmatrix} \frac{\partial}{\partial \mathrm{x}} & 0 \\ 0 & \frac{\partial}{\partial \mathrm{y}} \\ \frac{\partial}{\partial \mathrm{y}} & \frac{\partial}{\partial \mathrm{x}} \end{bmatrix} \begin{bmatrix} \varphi_1 & 0 & \dots & \varphi_n & 0 \\ 0 & \varphi_1 & \dots & 0 & \varphi_n \end{bmatrix} \begin{Bmatrix} u_1 \\ v_1 \\ \vdots \\ u_n \\ v_n \end{Bmatrix}$$

$$\boldsymbol{\varepsilon}_{(3\times1)} = \begin{bmatrix} \frac{\partial \varphi_1}{\partial \mathrm{x}} & 0 & \dots & \frac{\partial \varphi_n}{\partial \mathrm{x}} & 0 \\ 0 & \frac{\partial \varphi_1}{\partial \mathrm{y}} & \dots & 0 & \frac{\partial \varphi_n}{\partial \mathrm{y}} \\ \frac{\partial \varphi_1}{\partial \mathrm{y}} & \frac{\partial \varphi_1}{\partial \mathrm{x}} & \dots & \frac{\partial \varphi_n}{\partial \mathrm{y}} & \frac{\partial \varphi_n}{\partial \mathrm{x}} \end{bmatrix} \begin{Bmatrix} u_1 \\ v_1 \\ \vdots \\ u_n \\ v_n \end{Bmatrix}$$

$$\boldsymbol{\varepsilon}_{(3\times1)} = \mathbf{B}_{(3\times2n)}\mathbf{U}_{(2n\times1)} \quad (21)$$

where **B** is the strain matrix.

The stress vector using the constitutive equations for the material at the point X in the problem domain can be written as:

$$\boldsymbol{\sigma}_{(3\times1)} = \mathbf{D}_{(3\times3)}\boldsymbol{\varepsilon}_{(3\times1)}$$

$$\boldsymbol{\sigma}_{(3\times1)} = \mathbf{D}_{(3\times3)}\mathbf{B}_{(3\times2n)}\mathbf{U}_{(2n\times1)} \quad (22)$$

For an isotropic homogeneous material in the plane stress state, the matrix of material elastic constants **D** can be expressed as:

$$\mathbf{D} = \frac{\mathrm{E}}{1-\nu^2}\begin{bmatrix} 1 & \nu & 0 \\ \nu & 1 & 0 \\ 0 & 0 & \frac{1-\nu}{2} \end{bmatrix} \quad (23)$$

The traction **t** at a point X has the following form

$$\mathbf{t} = \begin{Bmatrix} \mathrm{t_x} \\ \mathrm{t_y} \end{Bmatrix} = \begin{bmatrix} \mathrm{n_x} & 0 & \mathrm{n_y} \\ 0 & \mathrm{n_y} & \mathrm{n_x} \end{bmatrix} \begin{Bmatrix} \sigma_{xx} \\ \sigma_{yy} \\ \tau_{xy} \end{Bmatrix}$$

$$\mathbf{t} = \mathbf{N}_{(2\times3)}\mathbf{D}_{(3\times3)}\mathbf{B}_{(3\times2n)}\mathbf{U}_{(2n\times1)} \quad (24)$$

In which $(\mathrm{n_x}, \mathrm{n_y})$ is the vector of the unit outward normal on the boundary.

We now change eq. (8) to the following matrix form to derive the discretized system equations in a matrix form:

$$\int_{\Omega_\mathrm{q}} \mathbf{W}_i{}^T\boldsymbol{\sigma}\, \mathrm{d}\Omega - \int_{\Gamma_\mathrm{q}} \boldsymbol{\Theta}_i{}^T\mathbf{t}\, \mathrm{d}\Gamma = \int_{\Omega_\mathrm{q}} \boldsymbol{\Theta}_\mathrm{i}{}^T\mathbf{b}\, \mathrm{d}\Omega \quad (25)$$

where $\boldsymbol{\Theta}_\mathrm{i}$ is a matrix of weight functions given by

$$\boldsymbol{\Theta}_\mathrm{i} = \begin{bmatrix} \Theta_\mathrm{i}(\mathrm{X}) & 0 \\ 0 & \Theta_\mathrm{i}(\mathrm{X}) \end{bmatrix} \quad (26)$$

$\mathbf{W}_\mathrm{i}$ is a matrix that collects the derivatives of the weight functions

$$\mathbf{W}_\mathrm{i} = \begin{bmatrix} \Theta_{i,x}(\mathrm{X}) & 0 \\ 0 & \Theta_{i,y}(\mathrm{X}) \\ \Theta_{i,y}(\mathrm{X}) & \Theta_{i,x}(\mathrm{X}) \end{bmatrix} \quad (27)$$

Substitution of eq. (22) and eq. (24) into eq. (25) the matrix form of eq. (25) can be written as:

$$(\mathbf{K}_i)_{2\times2n}(\mathbf{U})_{2n\times1} = (\mathbf{f}_\mathrm{i})_{(2\times1)} \quad (28)$$

U is the vector that collecting displacements for each node i of field nodal distribution included in the considered support domain.

The matrix $\mathbf{K}_i$ called the nodal stiffness matrix for each node i of field nodal distribution, which is computed by using

$$\mathbf{K}_i = \int_{\Omega_q} \mathbf{W}_i^{\mathrm{T}} \mathbf{D} \mathbf{B}\, d\Omega - \int_{\Gamma_q} \mathbf{\Theta}_i^{\mathrm{T}} \mathbf{N} \mathbf{D} \mathbf{B}\, d\Gamma \qquad (29)$$

The nodal force vector $\mathbf{f}_i$ with contributions from body forces applied in the problem domain:

$$\mathbf{f}_i = \int_{\Omega_q} \mathbf{\Theta}_i^{\mathrm{T}} \mathbf{b}\, d\Omega \qquad (30)$$

Using eq. (28) for all n_t distribution nodes in the entire problem domain, we obtain a total of $2n_t$ independent linear equations. Assembling all these $2n_t$ equations based on the global numbering system to obtain the final global system equations in the form

$$\begin{bmatrix} \mathbf{K_{11}} & \mathbf{K_{12}} & \cdots & \mathbf{K_{1(2n_t-1)}} & \mathbf{K_{1(2n_t)}} \\ \vdots & \vdots & \ddots & \vdots & \vdots \\ \mathbf{K_{(2i-1)1}} & \mathbf{K_{(2i-1)2}} & \cdots & \mathbf{K_{(2i-1)(2n_t-1)}} & \mathbf{K_{(2i-1)(2n_t)}} \\ \mathbf{K_{(2i)1}} & \mathbf{K_{(2i)2}} & \cdots & \mathbf{K_{(2i)(2n_t-1)}} & \mathbf{K_{(2i)(2n_t)}} \\ \vdots & \vdots & \ddots & \vdots & \vdots \\ \mathbf{K_{(2n_t)1}} & \mathbf{K_{(2n_t)2}} & \cdots & \mathbf{K_{(2n_t)(2n_t-1)}} & \mathbf{K_{(2n_t)(2n_t)}} \end{bmatrix} \begin{Bmatrix} u_1 \\ v_1 \\ \vdots \\ u_2 \\ v_2 \\ \vdots \\ u_{n_t} \\ v_{n_t} \end{Bmatrix} = \begin{Bmatrix} f_{1x} \\ f_{1y} \\ \vdots \\ f_{ix} \\ f_{iy} \\ \vdots \\ f_{n_t x} \\ f_{n_t y} \end{Bmatrix}$$

We obtain

$$\mathbf{K}_{(2n_t)(2n_t)} \mathbf{U}_{(2n_t \times 1)} = \mathbf{F}_{(2n_t \times 1)} \qquad (31)$$

where

$\mathbf{K}_{(2n_t)(2n_t)}$ is the global stiffness matrix for all n_t nodes in the entire problem domain,

$\mathbf{U}_{(2n_t \times 1)}$ is the global displacement vector that collecting the nodal displacements of all n_t nodes in the entire problem domain,

$\mathbf{F}_{(2n_t \times 1)}$ is the global body force vector assembled using the nodal body force vectors for all nodes in the entire problem domain.

NUMERICAL RESULTS AND DISCUSSION

In this section, we present a numerical study for elastostatic 2-D problem of a cantilever rectangular homogeneous isotropic plate (figure 2**)**. The plate has a unit thickness and hence a plane stress problem is assumed [25].

We consider the following node numbers $n_t = 55, 95, 175$ and 196, regularly distributed. The isotropic plate analyzed with different materials properties: Steel (E=210GP, ν=0.29, $\rho = 7860 kg/m^3$) Aluminum (E=70GP, ν=0.3,$\rho = 2707 kg/m^3$), Copper (E=128GP, ν= 0.33, $\rho = 8920 kg/m^3$; Zinc$\left(E = 78GP\,;\ \nu = 0.25;\ \rho = 7100 kg/m^3\right)$. In the process of this study, a rectangular support domain and rectangular quadrature domain are adopted and gauss quadrature (4x4) was used to evaluate the integrals, where the dimension of the background cell was consistent with the nodal distance.

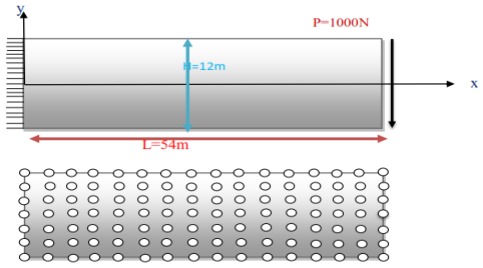

Figure 2: Configuration and nodal arrangement for the cantilever plate

Some important parameters on the performance of the method have been investigated. It has been found that the parameters α_s and α_q, which determines the size of the sub-domain needs to be chosen carefully, the results calculated by the LRPIM using Radial basis functions RBF-MQ (see table 1):

The dependence of energy error as a function of the shape parameter q for different types of considered materials (Steel, Aluminum, copper and zinc) and for the following node numbers $n_t = 55, 196$ regularly distributed is shown in figure 3. In this figure the value of α_c is fixed, we present the case $\alpha_c = 9.0$, the support domain adopted and is fixed at $\alpha_s = 3.0$. If the values of energy error between -2.0 and 2.8 the curves of each distribution of node number are identical form for all materials. The variation of energy error values with the shape parameter q is very little, and the domain of convergent is between -0.5 and 2.8 for $n_t = 55$ and between 0.0 and 2.8 for $n_t = 196$ but for q =1, 2 and 3 the LRPIM method is divergent. When q>2.8 for all materials and all distributions the error will significantly increase. We note that the energy error is small using the steel material compared with other materials used. Note that the domain of convergence is larger than that given in the references [16, 22]

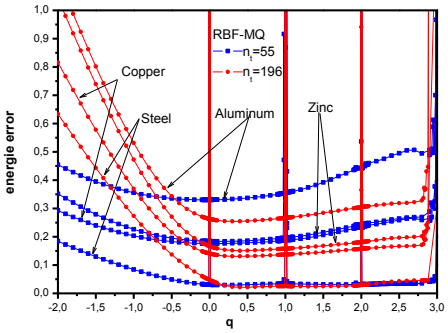

Figure 3: Variation of energy error as a function of shape parameter q using the fixed values; $\alpha_s = 3.0$, $\alpha_q = 2.0$ and $\alpha_c = 9.0$

Figure 4 displays the variation of energy error as a function of α_c for the following node numbers $n_t = 55, 95$ and 196 and different materials (Steel, Copper and Zinc). The results are obtained by using the values of $\alpha_q = 2.0$, q = 0.99 and $\alpha_s = 3.0$. We found that all curves of energy error falls from maximum values to the minimum values between α_c=3.0 and α_c=14 for $n_t = 55$ or between $\alpha_c = 3.0$ and α_c=12.3 for $n_t = 95$ and 12.0 for $n_t = 196$.

For the values of α_c greater than 14 for $n_t = 55$ and 12.3 for $n_t = 95$ and 12.7 for $n_t = 196$, the curves are not stable for all materials, and the LRPIM method is not convergent. The domain of convergence is very large and is between $\alpha_c = 4.0$ and 14 for $n_t = 55$, between 4.0 and 12.3 for n_t=95 and 196. We can also say that the domain of the convergence is broader than that given in the reference [16].

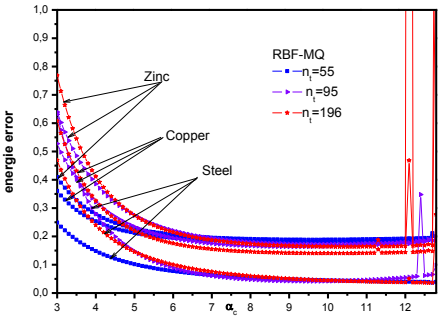

Figure 4: Variation of energy error as a function of shape parameter $\alpha_c$by using the fixed values ; $\alpha_s = 3.0$, $\alpha_q = 2.0$ and q=0.99

Figure 5 shows the energy error variation as a function of the size of support domain α_s. It is investigated the variation of maximum and minimum values of α_s convergence domain for different regular distribution node numbers. It can be seen from this figure for all materials (Steel, Aluminum, copper and zinc) that; if the values of α_s is smaller than 1.89, the energy error is large and LRPIM method is not convergent. The domain of convergence reaches the maximum value at $\alpha_s = 5$ for $n_t = 55$ and $\alpha_s = 3.66$ for $n_t = 196$. In this study the convergence domain for all materials is noticed to be between a small value $\alpha_s = 1.89$ and the maximum value $\alpha_s = 5$ for n_t=55 and the maximum value $\alpha_s = 3.66$ for the greater value of node number distribution $n_t = 196$. We can also say that the domain of the convergence is broader than that given in the reference [22].

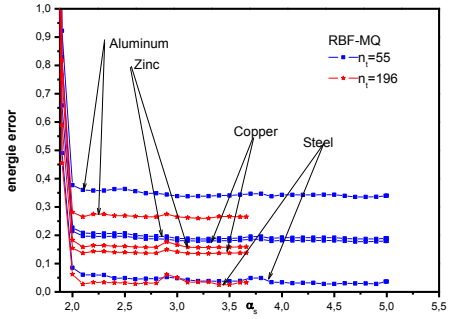

Figure 5: Variation of energy error as a function of size of support domain $\alpha_s$by using the fixed values ; α_q=2.0 α_c=9.0 and q=0.99

In figure 6 the variation of energy error as a function of the size of the local quadrature domain α_q for following node number $n_t = 55, 95, 196$ and different materials (Steel, Copper and Zinc) is plotted. The LRPIM method is convergent for the values of α_q ranging; between 1.3 and 2.6 using Steel for all node numbers and between 1.3 and 2.5 for $n_t = 95$ and 196, and between 1.3 and 2.4 for $n_t = 55$ using zinc and copper, but if the values of

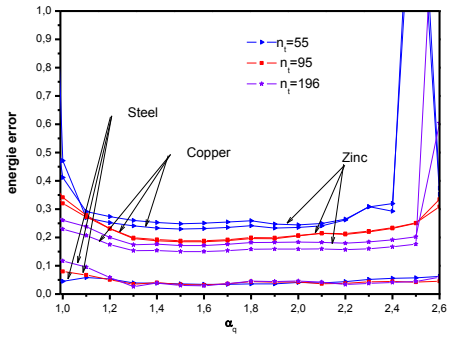

Figure 6: Variation of energy error as a function of size of quadrature domain α_q by using the fixed values $\alpha_s = 3.0$, q=2,03 and $\alpha_c = 9.0$

α_q is different this domains the energy error is very large and the LRPIM method is divergent. Note that the energy error using the Steel material is smaller comparing with that obtained by using zinc and copper.

In the next paragraph the results are calculated by the RPIM using Radial Basis Functions TPS (**table 1**) for different distributions of node numbers using different materials **(**Steel, Aluminum, Copper and Zinc).

Figure 7 illustrates the effect of different materials using two distributions of node numbers $n_t = 175$ and 196 on shape parameter η with fixed values of α_s and α_q ($\alpha_s = 3.0, \alpha_q = 2.0$).The obtained curves are identical for all materials and for all node numbers. Significant results can be obtained when the

value of η varies between 3.998 and 4.002.The value η = 4.0001 leads to the best result.

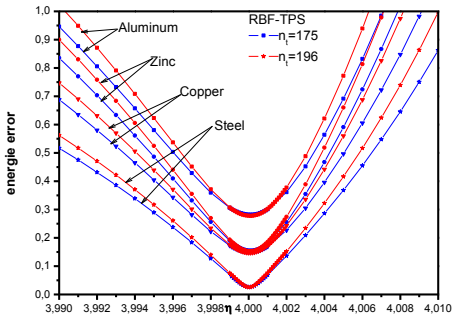

Figure 7: Variation of energy error as a function of shape parameter η by using the fixed values ; $\alpha_s = 3.0$ and $\alpha_q = 2.0$

The effect of the size of support domain α_s for different distribution of nodes using different materials is gives in figure 8 with the fixed values ; $\eta = 4.0001$, $\alpha_q = 2.0$. We find that the curves of all materials are identical for each value of node numbers n_t, and the value of energy error is smaller using steel material and it is greater using Copper and Zinc for all distribution of nodes. The domain of convergence reaches the maximum value at $\alpha_s = 5$ for $n_t = 55$ and $\alpha_s = 3.66$ for $n_t = 91$ and 196. For all materials the convergence domain is noticed to be between a small value $\alpha_s = 1.89$ for all distributions of nodes and the greater values $\alpha_s = 5$ for $n_t = 55$ and $\alpha_s = 3.66$ for the node numbers $n_t = 91$ and 196.

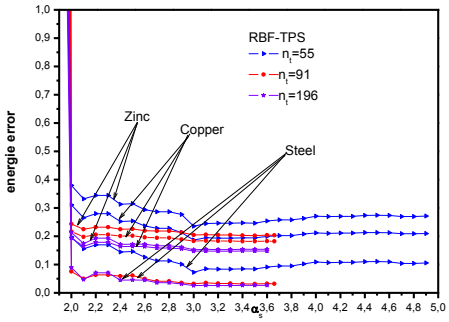

Figure 8: Variation of energy error as a function of size of support domain α_s by using the fixed values ; $\alpha_q = 2.0$ and $\eta = 4.0001$

The influence of the size of quadrature domains α_q for tow distribution of nodes n_t=175 and 196 using different materials is plotted in figure 9. In this study the values of η and α_s are fixed ($\eta = 4.0001$ and $\alpha_s = 3.0$). We note that the energy error is smaller for steel in comparison with other materials and the obtained curves for two distribution of nodes n_t=175 and 196 and for all materials are very stable between $\alpha_q = 0.5$ and $\alpha_q = 2.5$ and the convergence domain is very wide and it is between $\alpha_q = 0.5$ and $\alpha_q = 2.5$ for all materials.

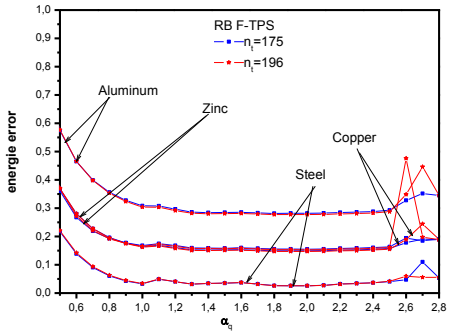

Figure 9: Variation of energy error as a function of size of quadrature domain α_q using the fixed values ; $\alpha_s = 3.0$ and $\eta = 4.0001$

In figure 10, the displacement results are plotted as a function of x with y =0 for different materials and with fixed values of; size of quadrature domain $\alpha_q = 2.0$ and size of support domain $\alpha_s = 3.0$. The shape parameters of the considered radial basis function; RBF-MQ are $\alpha_c = 9.0$ and $q = 0.98$ and RBF-TPS is $\eta = 4.0001$. The effect of different Young's modulus E on the displacement values is presented in this figure, we note that the curves found using Radial Basis Functions MQ and TPS are identical for each material and each curve is identical to analytical value.

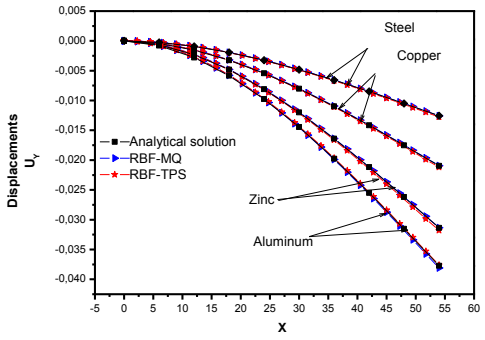

Figure 10 : Displacement u_y distribution along the Y axis usiug RBF with MQ and TPS for different materials with $\alpha_s = 3.0$, $\alpha_q = 2.0$, $\alpha_c = 9.0$ and q=2.03

CONCLUSIONS

In this paper, the pure meshfree Local Radial Point Interpolation Method (LRPIM) for 2D dimensional elastostatic plate is presented. Two Radial Basis Functions RBF-MQ and RBF-TPS are used to construct shape functions based on a 2D local support domain. Some important parameters are investigated in detail and the numerical example of different materials (different values of (E and ν)) are studied using the present LRPIM method. We note that energy error is small using steel plate compared with other materials and it's

confirmed that, no effect of E and ν on convergence of LRPIM method.

Comparatively with references [15, 16], we can conclude that the convergence domain of shape parameters of RBFs basis is significant. Concerning the sizing parameter α_s of support domain, the domain of convergence for the different distribution of nodes used, decreases if the number of nodes increases, we find that for the small values of distribution node numbers $\alpha_s = 5.0$ and for the greater values of node number distributions α_s is decreasing ($\alpha_s = 3.66$).

REFERENCES

[1] KANSA E. J., (1990-I). Multiquadrics-a scattered data approximation scheme with applications to computational fluid-dynamics-I. Surface approximations and partial derivative estimates ; Computer Math. Applic. Great Britain : 19, 8/9, 127-145.

[2] Gingold R. A. and Monaghan J. J., 1977. Smoothed particle hydrodynamics: theory and application to non-spherical stars, Mon. Not. R. astr. Soc. 181, 375-389.

[3] Nayroles B., Touzot G., Villon P., 1992. Generalizing the finite element method: diffuse approximation and diffuse elements, Comput. Mech., 10, 307–318.

[4] Belytschko T., Lu Y., Gu L., 1994. Element-free Galerkin methods, International Journal for Numerical Methods in Engineering, 37, 229–256.

[5] Xiao Lin Li and Li Ming Zhou, 2017. An element-free Galerkin method for electromechanical coupled analysis in piezoelectric materials with cracks, Advances in Mechanical Engineering, 9(2), 1-11.

[6] Liu W., Jun S., Zhang Y., 1995. Reproducing kernel particle methods, International Journal for Numerical Methods in Fluids, 20, 1081–1106.

[7] Li S. C. and Cheng Y. M., 2004. "Meshless numerical manifold method based on unit partition," Acta Mechanica Sinica, vol. 36, no. 4, pp. 496–500.

[8] Duarte C. A., Oden J. T., 1996. Hp clouds—a meshless method to solve boundary value problems, Computational Methods in Applied Mechanics and Engineering, 139, 237–262.

[9] Onnate E., Idelsohn S., Zienkiewicz O. C., Taylor R. L., 1996. A finite point method in computational mechanics, Application to convective transport and fluid flow, Int. J. Numer. Meth. Engrg., 39, 3839–3866.

[10] Atluri S. N., 2004. The Meshless Local Petrov-Galerkin (MLPG) Method for Domain & Boundary Discretizations, Tech Science Press.

[11] Liszka T., 1984. An interpolation method for an irregular net of nodes, Int. J. Numer. Meth. Engrg., 20, 1599–1612.

[12] Xiao J. R., McCarthy M. A., 2003. A local Heaviside weighted meshless method for two-dimensional solids using radial basis functions, Computational Mechanics, 31, 301–315.

[13] Chen, J. S., Belytschko, T., 2015. Meshless and Meshfree Methods, Encyclopedia of Applied and Computational Mathematics , Springer-Verlag, Berlin, Heidelberg, 886-894.

[14] Bao-Jing Zheng, Xiao-Wei Gao, Kai Yang, Chuan-Zeng, 2015. A novel meshless local Petrov–Galerkin method for dynamic coupled thermoelasticity analysis under thermal and mechanical shock loading, Engineering Analysis with Boundary Elements, 60, 154-161.

[15] Liu G. R. , Zhang G. Y., Wang Y. Y. , Zhong Z. H. , Li G. Y., Han X., 2007. A nodal integration technique for meshfree radial point interpolation method (NI-RPIM), International Journal of Solids and Structures, 44, 3840–3860.

[16] Wang J. G., Liu G. R., 2002. On the optimal shape parameters of radial basis functions used for 2-D meshless methods. Comput. Meth. Appl. Mech. Eng., 191, 2611–2630.

[17] Liu G. R., Zhang G. Y., Gu Y. T., Wang Y. Y., 2005. A meshfree radial point interpolation method (RPIM) for three-dimensional solids, Comput. Mech., 36, 421–430.

[18] Xiao J. R., McCarthy M. A., 2003. A local Heaviside weighted meshless method for two-dimensional solids using radial basis functions, Computational Mechanics, 31, 301–315.

[19] Liu G. R. , Zhang G. Y. , Y. Y. Wang , Zhong Z. H., Li G. Y., Han X., 2007. A nodal integration technique for meshfree radial point interpolation method (NI-RPIM), International Journal of Solids and Structures, 44:3840–3860.

[20] Zhang X., Song K. Z., Liu X., 2000. Meshless methods based on collocation with radial basis functions. Computational Mechanics, 26, 333–343.

[21] Gu Y. T., Liu G. R., 2001. A local point interpolation method for static and dynamic analysis of thin beams. Comput. Meth. Appl. Mech. Eng., 190, 5515–5528.

[22] Liu G. R. , Gu Y. T., 2001. A local radial point interpolation method (LR-PIM) for free vibration analyses of 2-D solids ; J. of Sound and Vibration, 246, (1), 29-46.

[23] Liu G. R., Gu Y. T., 2002. A boundary point interpolation method for stress analysis of solids ; Computational Mechanics, 28, 47-54.

[24] Victor Katz J., 1979. The History of Stokes Theorem, Mathematical Association of America, 52, 146-156.

[25] Timoshenko S. P., Woinowsky-Krieger K., 1959. Theory of Plates and Shells (McGraw-Hill, New

York).

[26] Dağ İ., Dereli Y., 2008. "Numerical solutions of KdV equation using radial basis functions," Applied Mathematical Modelling, 32, 4 535–546

[27] Kanber B., Bozkurt O. Y., Erklig A.. 2013. Investigation of RPIM shape parameter effects on the solution accuracy of 2D elastoplastic problems. Int J Comput Meth Eng Sci Mech 14, 354-366.

[28] Dehghan M., Shokri A., 2008. A numerical method for solution of the two-dimensional sine-Gordon equation using the radial basis functions, Math. Comput. Simul. 79, 700–715.